ISSN 0965-5441, Petroleum Chemistry, 2022, Vol. 62, No. 10, pp. 1162–1170. © Pleiades Publishing, Ltd., 2022.
ISSN 0965-5441, Petroleum Chemistry, 2022. © Pleiades Publishing, Ltd., 2022.
Russian Text © The Author(s), 2022, published in Neftekhimiya, 2022, Vol. 62, No. 6, pp. 859–869.

Application of In Situ ATR-FTIR Spectroscopy for Determination of Wax Appearance Temperature at High-Pressure CO_2 Conditions

A. S. Shalygin[a,b,*], E. V. Morozov[b,c], and O. N. Martyanov[a]

[a] *Boreskov Institute of Catalysis, Siberian Branch of Russian Academy of Sciences (BIC SB RAS), Novosibirsk, 630090 Russia*

[b] *Institute of Chemistry and Chemical Technology, Siberian Branch of Russian Academy of Sciences (ICCT SB RAS), Krasnoyarsk Scientific Center SB RAS, Krasnoyarsk, 660036 Russia*

[c] *L.V. Kirensky Institute of Physics, Siberian Branch of Russian Academy of Sciences, Krasnoyarsk Scientific Center SB RAS, Krasnoyarsk, 660036 Russia*

**e-mail: shas@catalysis.ru*

Received September 21, 2022; revised November 14, 2022; accepted December 8, 2022

Abstract—Attenuated total reflection Fourier-transform infrared (ATR-FTIR) spectroscopy was for the first time employed to investigate in situ paraffin crystallization under CO_2 high-pressure and to evaluate a critical parameter—wax appearance temperature (WAT). To determine the WAT under pressure, conventional calculation methods based on changes in the band of rocking vibrations of CH_2 group were used. Using model 10 wt % paraffin solutions in *n*-dodecane, temperature effects were investigated under CO_2 pressures of 10, 20, 30, and 40 atm. It was experimentally confirmed that an increase in the CO_2 pressure reduces the WAT. Furthermore, the plot of peak intensity of the spectral band attributed to dissolved CO_2 as a function of temperature showed a maximum that can serve as an additional WAT indicator. This enhances the measurement accuracy and the reliability of WAT evaluation.

Keywords: ATR, FTIR spectroscopy, paraffins, wax appearance temperature (WAT), CO_2 pressure

DOI: 10.1134/S0965544122100176

Despite the rapid advances in alternative energy sources, the worldwide consumption of liquid fossil fuels continues to increase [1]. Therefore, it has become increasingly relevant to develop methods for more complete recovery of crude oils.

In terms of reservoir pressure types and oil recovery techniques, oil production methods can be divided into primary, secondary, and tertiary. Primary oil recovery is based on natural drive mechanisms. Secondary recovery—a technique that uses steam and gas injection—is employed when primary production no longer provides the desired performance. However, both primary and secondary techniques are known to recover no more than about 30–50% of crude oil from reservoirs [2, 3]. This has motivated the development and application of tertiary methods, also known as enhanced oil recovery (EOR), capable of increasing oil recovery up to 70% or even higher [4, 5]. EOR methods can basically be divided into three main approaches: gas injection; in situ heating of crude oil (to lower its viscosity); and chemical injection of mineralized water, gas mixtures, alkali liquors, etc. Current research mostly focuses on gas injection as the most promising approach [6].

Various gases, such as flue gases, nitrogen, natural gas, and CO_2, are generally used for gas drive, of which CO_2 appears the most promising [7]. Carbon dioxide has a good track record due to its high reservoir sweep efficiency; in addition, CO_2 disposal contributes to the reduction of greenhouse gas emissions [8]. However, the use of carbon dioxide for enhanced oil recovery (CO_2-EOR) faces the challenge of uncontrolled deposits, thus potentially decreasing the permeability of the rock (due to blockage of voids) and/or affecting the wetting of the rock's surface [9]. Thus, using CO_2 can sometimes

impair the oil recovery efficiency as a whole, as well as hamper further use of the wells and entire oil reservoirs.

The deposits resulting from oil production mostly consist of asphaltenes and high-molecular-weight paraffins. However, unlike abundant research into CO_2 effects on resin-asphaltene deposition [10–12], the effects of CO_2 on the behavior of oil-dissolved paraffins have been underexplored. While there are available reports on binary and ternary phase equilibriums of *n*-alkanes and phase diagrams for pure components [13–16] in the presence of CO_2, there are nearly no research data on the phase behavior of complex paraffin mixtures and the CO_2 effects on paraffin precipitation.

The lack of data can be explained by the limited applicability of existing characterization methods for paraffinous systems, such as visual observation, differential scanning calorimetry (DSC), viscometry, cross-polarization microscopy, etc. Most of them can operate only at atmospheric pressure, so that they require substantial modification to fit higher pressures. For example, high-pressure DSC (HPDSC) was used to characterize CO_2 pressure effects on the wax appearance temperature (WAT) of some crude oils [17]. Studies of *n*-alkanes–CO_2 systems [13–16] carried out using visual control methods were supplemented by subsequent thermodynamic modeling. In particular, phase equilibria were studied under CO_2 pressure for C_{10}/C_{20}, C_{10}/C_{24}, and $C_{10}/C_{20}/C_{24}$ *n*-alkane mixtures [15], and for $C_{12}/C_{16}/C_{22}/C_{23}/C_{24}$ *n*-alkane mixtures [16].

FTIR spectroscopy has been extensively used to investigate *n*-alkanes and phase transitions in their mixtures [18–20]. Nonetheless, there are no reports on the employment of this method to study the phase behavior of paraffins under CO_2 pressure. On the other hand, a modification of this method—namely, attenuated total reflection FTIR (ATR-FTIR) spectroscopy—has enabled researchers to obtain good results when examining systems in situ, i.e. over the course of direct real-time observation of relevant variations or transformations, including under high gas pressure conditions [21–24]. The relatively easy sample preparation procedure and simple installation of pressure equipment based on ATR diamond prisms offer a number of important advantages: operability with a small optical path length (1–10 μm), avoiding the need to seal the windows; recording spectra of dense gases and strongly-absorbing objects without exceeding the spectrometer's intensity limits; and adequate operating safety ensured by the small volume of the high-pressure cell [25]. ATR-FTIR spectroscopy has been extensively used in research on the behavior of polymers under CO_2 pressure, including supercritical conditions [26, 27], and is readily applicable for in situ studies of CO_2-induced asphaltene precipitation [22].

The above advantages make this method beneficial for the investigation of the phase behavior of paraffins in the presence of CO_2.

The purpose of this study was to demonstrate an ability to measure the WAT under CO_2 high-pressure by in situ ATR-FTIR spectroscopy.

EXPERIMENTAL

A number of samples that contained paraffins (10 wt %, mp 53–57°C, Sigma Aldrich, USA) dissolved in *n*-dodecane (90 wt %, AR grade, NevaReaktiv, Russia) were prepared. Carbon dioxide was purchased from Pure Gases, Novosibirsk, Russia. The molecular composition of the paraffins is shown in Fig. 1.

Initially, the WAT of the paraffins dissolved in *n*-dodecane was independently measured by viscometry on an SV-10A vibration viscometer (A&D, Japan) equipped with a cell in which the temperature was adjusted by a *M01M* external thermostat (Termex, Russia).

At high temperatures, when paraffins are completely dissolved, their viscosity–temperature relationship is known to fit a linear Arrhenius plot ($\ln \eta$ vs. $1/T$) [28]. Under cooling, however, as paraffin solids appear in the solution, the slope of the linear plot markedly changes (Fig. 1b). This change enabled us to find with high accuracy that the WAT for the system under study was 24.5°C.

Next, the WAT was measured by ATR-FTIR spectroscopy using a Vertex 70V FTIR spectrometer (Bruker, Germany) with a cooled MCT detector. The detector was equipped with a high-temperature Golden Gate ATR accessory (Specac, UK) with a diamond prism and a USB controller capable of temperature control with an accuracy of ±0.1°C. ATR-FTIR spectra were recorded in situ at a resolution of 2 cm^{-1}, with the number of scans varying from 64 to 128. To record spectra under high gas pressure, we used a steel cell pressed around the measuring surface of the ATR diamond prism and fitted with a teflon gasket. The cell was held in place using a clamp attached into the Golden Gate accessory (Fig. 2). The gas pressure was controlled by an ISCO

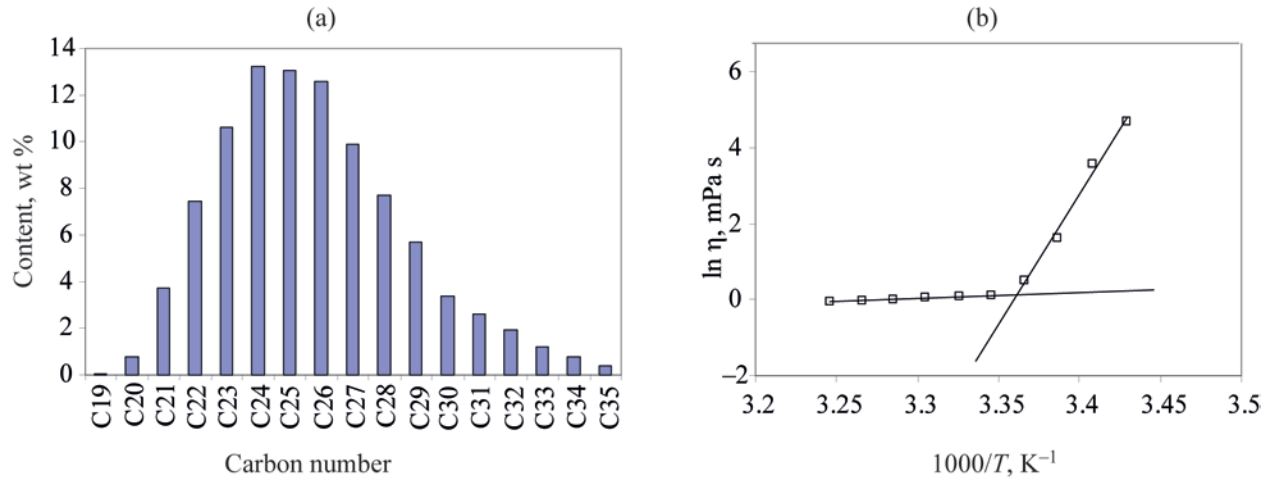

Fig. 1. (a) Molecular composition of paraffin samples (mp 52–57°C); and (b) viscosity Arrhenius plot (ln η vs. inverse temperature) for 10 wt % paraffin solution, with WAT indicated by the intersection of lines.

D260 syringe pump (Teledyne, USA) with an accuracy of 0.5% of the full scale of the pressure gauge. The accessory was cooled by cooling a steel plate into which the ATR diamond prism was embedded. Aluminum heat exchangers connected to a FT-316-40 thermostat (LOIP, Russia) through copper tubes were fixed on the steel plate surface. For better cooling, all connections were lubricated with thermal paste.

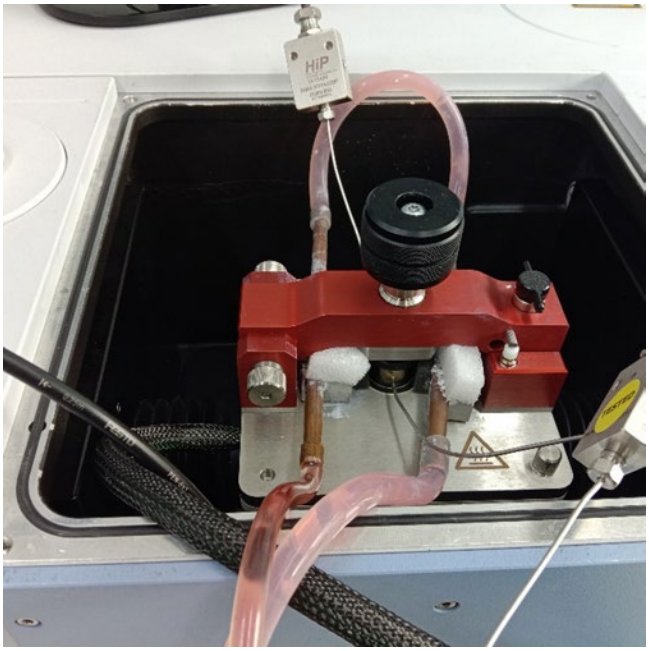

Fig. 2. Golden Gate ATR accessory in the FTIR spectrometer's sample compartment with heat exchangers installed and a high-pressure cell pressed against the ATR prism surface.

A cooled *n*-dodecane paraffin solution sample was placed in a high-pressure steel cell which was pressed to the measuring surface of the ATR diamond prism. The system was then heated until the paraffin solution turned completely homogeneous, upon which the gas was delivered to reach 10 to 40 atm as required. The system was held for about 30–50 min until the gas was completely dissolved according to the ATR-FTIR spectra. After this, the system was cooled, under temperature control, in 1–4°C increments. At each temperature, the solution was held for 20–40 minutes to reach an equilibrium state.

RESULTS AND DISCUSSION

Before the characterization of the paraffin solution under CO_2 pressure, relevant ATR-FTIR spectra were recorded at atmospheric pressure and various temperatures. The ATR-FTIR spectra of the paraffin solution at 33 to 12°C are shown in Fig. 3. The spectra of normal paraffins have a series of C–H stretching bands (3000–2800 cm^{-1}). The bands at 2957 and 2872 cm^{-1} are typical of asymmetric and symmetric C–H stretching vibrations in CH_3 groups, and bands at 2921 and 2823 cm^{-1} are attributable to identical vibrations in CH_2 groups (Fig. 3b). A series of bands typical of CH_3 and CH_2 bending vibrations appear in the region of 1520–1350 cm^{-1}: CH_2 symmetric bending vibrations

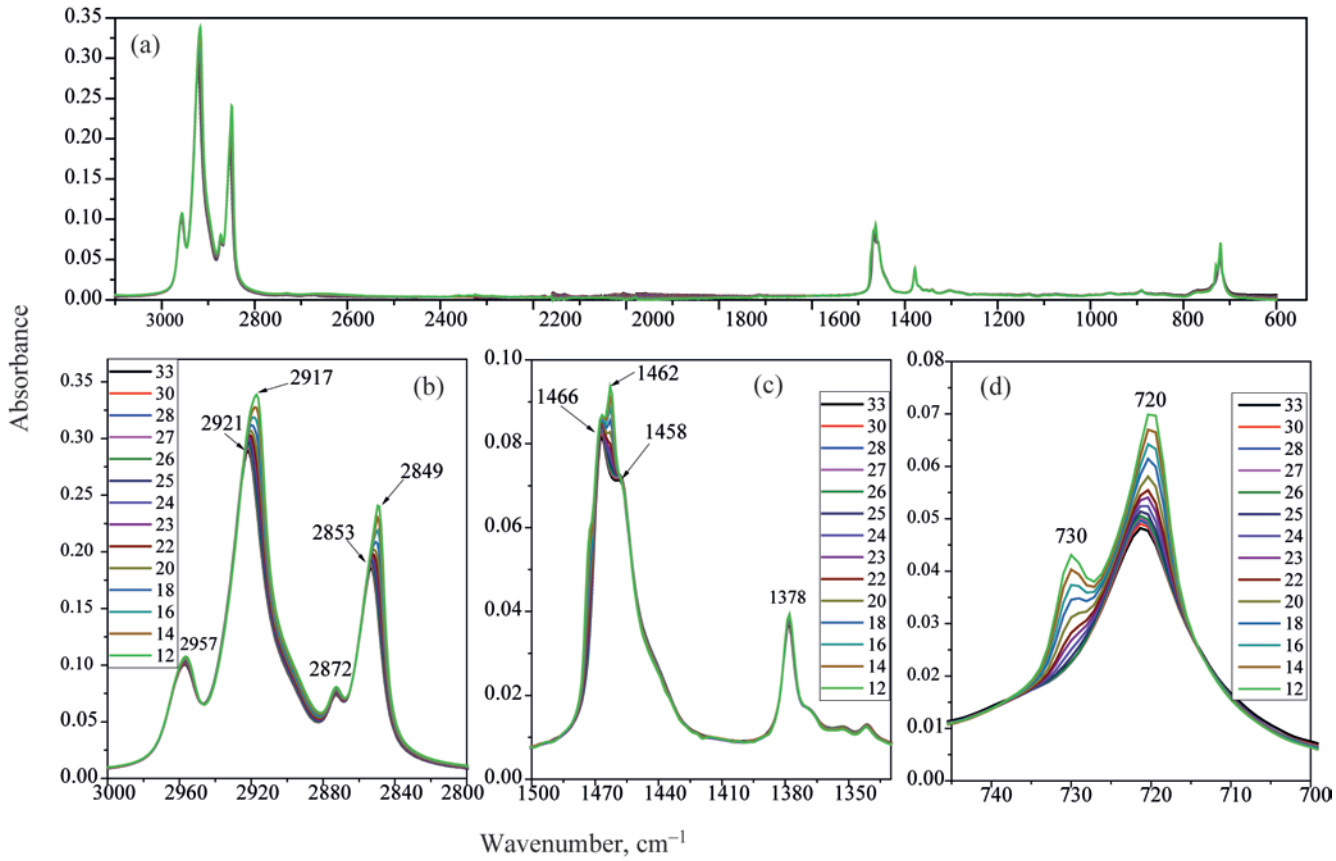

Fig. 3. ATR-FTIR spectra of 10 wt % paraffin solution in *n*-dodecane at different temperatures.

(1467 cm^{-1}) and CH_3 asymmetric and symmetric bending vibrations (1458 and 1378 cm^{-1}, respectively) (Fig. 3c). Furthermore, the spectra indicate absorption in the region of 750–700 cm^{-1}, attributed to CH_2 rocking modes (Fig. 3d).

The cooling of the paraffin solution affected both the locations and intensity of CH_2 bands. For example, the asymmetric and symmetric stretching bands of CH_2 groups shifted from 2921 and 2853 cm^{-1} to 2917 to 2849 cm^{-1}, respectively, with their intensities increasing (Fig. 3b). The CH_2 bending band changed, and a new band appeared at 1462 cm^{-1}, their intensity increasing with cooling (Fig. 3c). The most significant changes were observed for CH_2 rocking modes: a new band appeared at 730 cm^{-1} (Fig. 3d). All these IR spectral changes, typical of paraffin transition from a liquid to solid state, have been described and explained in detail in prior studies [29, 30]. This makes it possible to use any specific IR spectral variations for accurate identification of phase transition temperatures for paraffins and paraffin-containing systems: petroleum paraffins [31], bitumens [32], and asphalt binders [33].

After obtaining the reference data (without CO_2), the spectral changes of the paraffin solution were characterized in the CO_2 atmosphere at specific pressures and temperatures. Figure 4 provides the ATR-FTIR spectra of the paraffin solution at 34°C and atmospheric pressure (without CO_2), compared to the spectra under CO_2 pressures of 10, 20, 30, and 40 atm. In the CO_2 atmosphere, two additional bands corresponding to dissolved CO_2 appeared, specifically at 2335 cm^{-1} (ν_3, C=O asymmetric stretching vibrations) and 659 cm^{-1} (ν_2, O=C=O bending vibrations). The decrease in the absorbance of the paraffin solution bands indicates that CO_2 was absorbed by the solution. The wavenumbers of the ν_3 and ν_2 bands coincide with the data on CO_2 absorption by polyethylene [34] and are very close to the values for CO_2 absorption by polybutadiene (2334

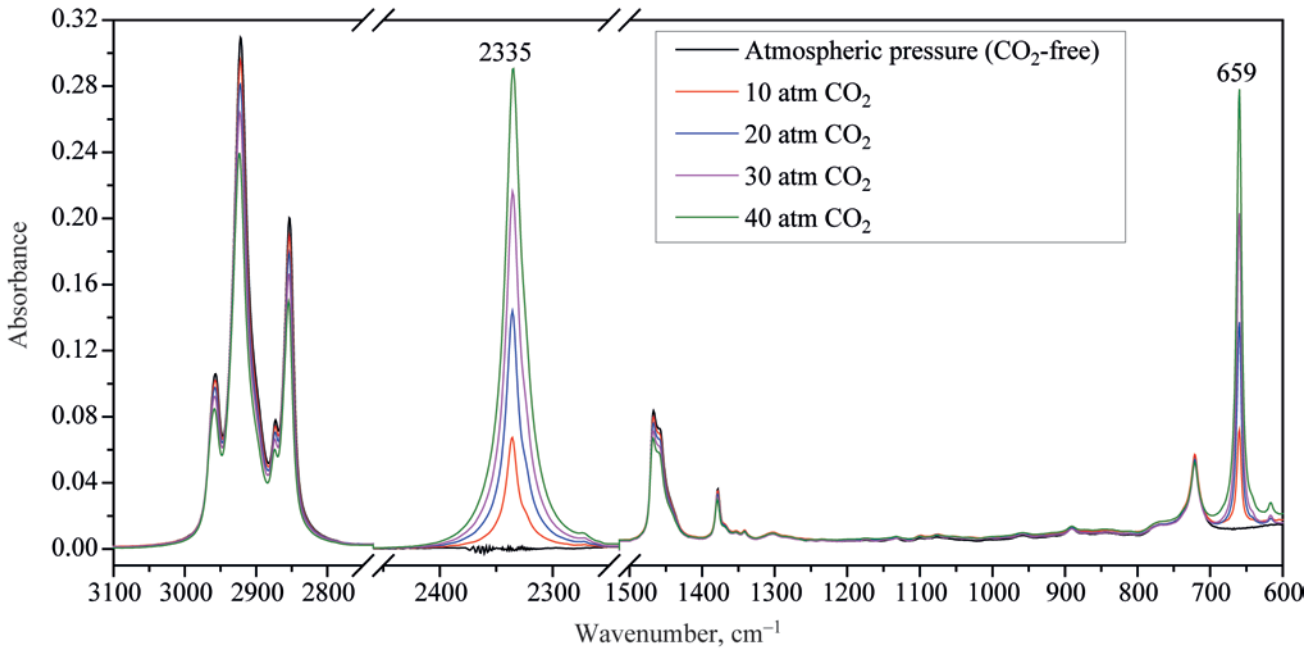

Fig. 4. ATR-FTIR spectra of paraffin solution in *n*-dodecane at 34°C for atmospheric pressure (CO_2-free) and CO_2 pressures of 10–40 atm. The CO_2 antisymmetric stretching (ν_3, at ca. 2335 cm^{-1}), bending (ν_2, at 659 cm–1) bands are observed.

and 657 cm^{-1}) [35]. In addition, no split of the ν_2 band was observed, unlike the cases of absorption by polymers or functionalized materials (e.g., with carbonyl groups) [34, 35]. This confirms that CO_2 molecules did not interact with paraffin or *n*-dodecane molecules.

Figure 5 presents the ATR-FTIR spectra of the paraffin solution at 30 atm CO_2 and different temperatures. The regions of C–H stretching vibrations, C=O stretching vibrations, CH_3 and CH_2 bending vibrations, and CH_2 rocking vibrations are shown separately (Figs. 5a, 5b, 5c, and 5d, respectively). In a manner similar to the CO_2-free paraffin solution case (at atmospheric pressure), cooling the paraffin solution in the CO_2 atmosphere at 30 atm affected both the position and intensity of the bands attributed to CH_2 groups. In particular, we see a shift of the absorption bands for C–H stretching vibrations (Fig. 5a) and the appearance of new bands in the regions of bending vibrations (1462 cm^{-1} in Fig. 5c) and rocking vibrations (730 cm^{-1} in Fig. 5d). However, an important difference between these spectra and those at atmospheric pressure should be emphasized: under CO_2 pressure, the spectral changes manifested themselves at lower temperatures. Furthermore, the cooling increased the intensity of the C=O stretching band, the maximum being reached at 23°C.

The WAT was derived from the change in the CH_2 rocking vibration band (720 cm^{-1}). For this purpose, the integral intensity of this peak was plotted as a function of temperature in the range of 735–715 cm^{-1}. The WAT was determined as the temperature at which the slope of integral intensity vs. temperature changed [36]. Based on the linear dependence of integral intensity on the amount of solid hydrocarbons [37], the authors of [36] proposed a quantitative method for evaluating the amount of precipitated paraffins for crude oils and showed a good correlation with the centrifugation method. A US patent [38] describes a method for calculating a reduced spectral area as a ratio of the integrated spectral area of the 735–715 cm^{-1} band (S2) to the integrated spectral area of the 1402–1324 cm^{-1} band (S1). This method ensures that possible uncontrolled errors of FTIR spectra (caused by fluctuations in sample locations, temperatures, or other spectrometer instabilities) are properly eliminated. The thing is that the 1402–1324 cm^{-1} bands attributable to CH_3 bending vibrations are insensitive to the temperature of the sample.

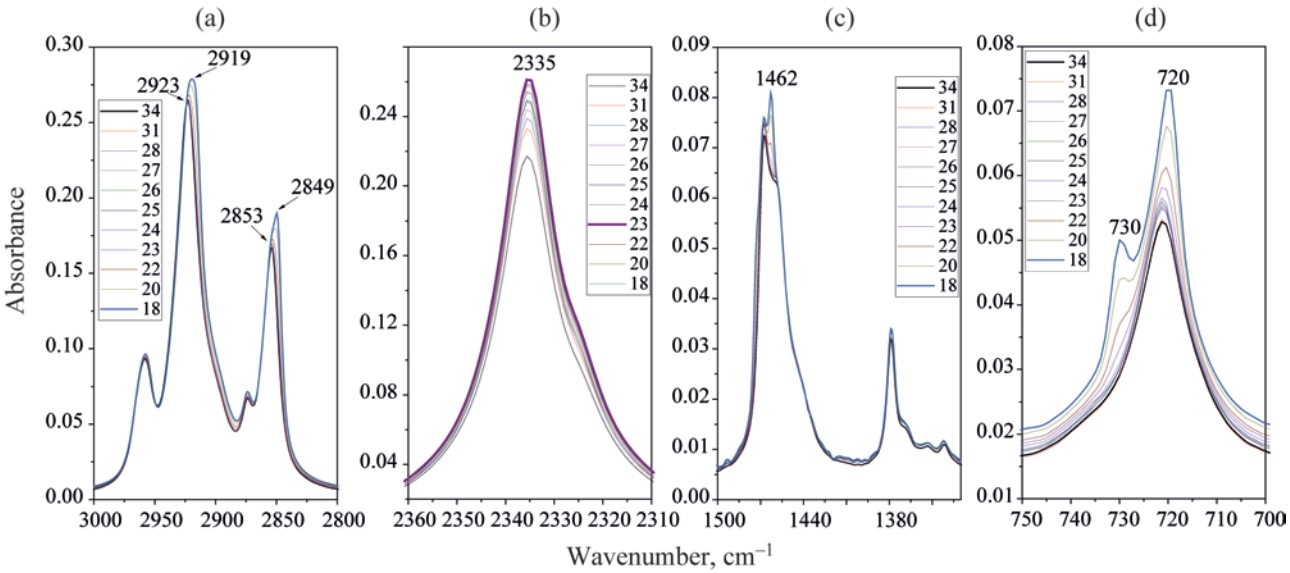

Fig. 5. ATR-FTIR spectra of 10 wt % paraffin solution in *n*-dodecane under 30 atm CO_2 at different temperatures.

Figure 6 shows the S2/S1 ratio as a function of temperature for the paraffin solution at atmospheric pressure (without CO_2) and CO_2 pressures of 10, 20, 30, and 40 atm. In all cases we see two regions where the experimental data points can be approximated by a straight line. The intersection point of the two lines is the wax appearance temperature. At atmospheric pressure and 10 atm CO_2, the WAT equaled 25.6°C, slightly higher than the value identified by viscometry (24.5°C). This difference can be explained by the fact that solids formed in the system need to account for about 1% to ensure that variations in the solution viscosity are safely recorded, whereas FTIR spectroscopy and DSC have higher sensitivity to the formation of primary paraffin crystals, thus giving higher WAT values [28].

At 20, 30, and 40 atm CO_2, the WAT was 24.4, 23.6, and 22.3°C, respectively. Therefore, the WAT decrease with a increase in the CO_2 pressure. These data are in good agreement with a published report on a WAT decrease in response to an increase in carbon dioxide pressure in crude oils [17]. Our data are also consistent with available thermodynamic modeling data for binary and ternary systems that contain paraffins and *n*-alkanes in the presence of CO_2 [15, 16]. Thus, in situ high-pressure ATR-FTIR spectroscopy is a reliable method for evaluating the wax appearance temperature.

Special mention should be made of the intensity trends with CO_2 dissolved in the system. Figure 7 provides

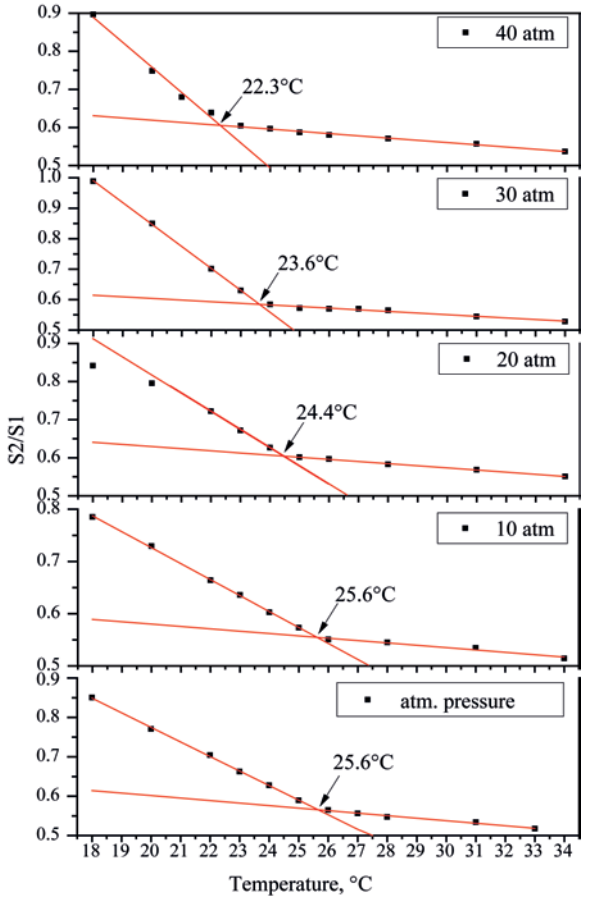

Fig. 6. Dependence of the S2/S1 ratio on temperature for paraffin solution at atmospheric pressure and 10, 20, 30, 40 atm CO_2.

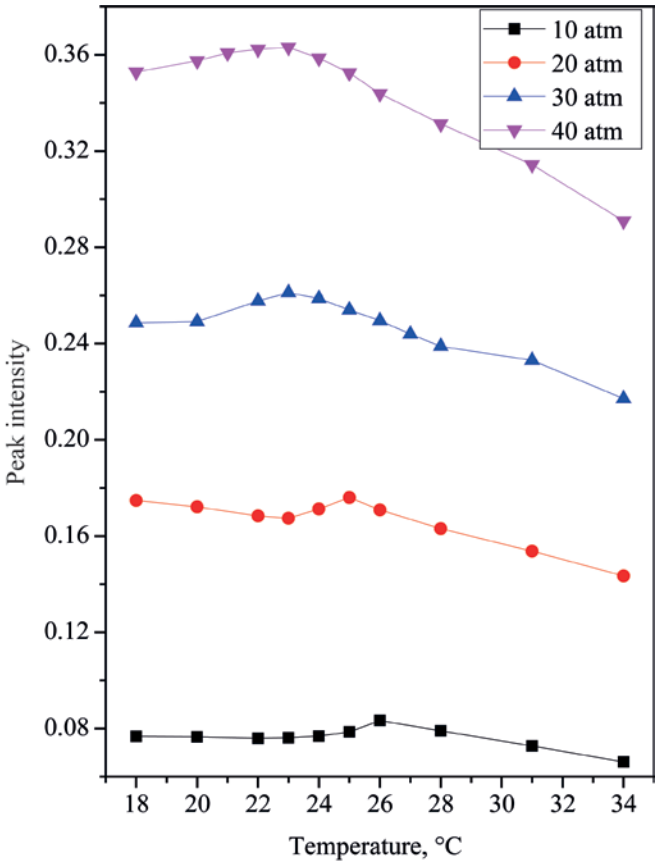

Fig. 7. Dependence of the peak intensity of the band stretching vibrations of CO_2 on temperature at 10, 20, 30, and 40 atm CO_2.

a plot of peak intensity of the CO_2 stretching band as a function of temperature at different CO_2 pressures (10, 20, 30, and 40 atm). The cooling led to an increase in the band intensity, evidently due to the rise in CO_2 solubility. The maximum observed on all the curves near the WAT are likely associated with the ATR-FTIR spectra recording procedure. In the ATR mode, the IR radiation is known to penetrate the sample to a certain depth (referred to as effective thickness), and this depth depends on various parameters such as the refractive indices (RI) of the ATR prism and the tested sample, the IR beam incidence angle with respect to the prism–sample contact plane, and the incident wavelength. All these parameters are included in the effective thickness equation [39]. For example, for *n*-dodecane (RI 1.4216; the beam angle for the given ATR accessory is 45°), the effective thickness is 1.36 and 4.35 μm for wavenumbers of 2335 and 730 cm^{-1}, respectively. Available reports lack any evidence of CO_2 solubility in solid paraffins at the pressures used in our study. Thus, the CO_2 band intensity decrease can be explained by the generation of paraffin microcrystals and, hence, by a decrease in the relative CO_2 concentration in the effective thickness. Accordingly, the maximum on the CO_2 peak intensity curves can also be used as a WAT indicator.

CONCLUSIONS

In the present study, in situ ATR-FTIR spectroscopy was for the first time employed for direct experimental measurement of wax appearance temperature under CO_2 high-pressure. This method proved to be effective.

The proposed method confirmed a WAT decrease as the CO_2 pressure was elevated. This finding is in good agreement with published thermodynamic modeling data on the phase behavior of *n*-alkane mixtures. Furthermore, the intensity of CO_2 absorption bands was found to decrease under cooling below the WAT. It is known from the literature that paraffin microcrystals formed below WAT are not contain of dissolved CO_2. Therefore, the pattern observed is likely associated with the fact that the paraffin microcrystals formed within the effective IR penetration depth reduce the apparent CO_2 concentration, as indicated by the decreasing intensity of CO_2 absorption bands in the ATR-FTIR spectra. The study results demonstrate the applicability and reliability of the proposed approach for practical improvement of the performance of EOR methods.

AUTHOR INFORMATION

A.S. Shalygin, ORCID: https://orcid.org/0000-0002-7414-4256

E.V. Morozov, ORCID: https://orcid.org/0000-0003-1561-3937

O.N. Martyanov, ORCID: https://orcid.org/0000-0001-9999-8680

FUNDING

This study was funded by the Russian Science Foundation (project no. 21-13-00171, http://rscf.ru/project/21-13-00171/).

CONFLICT OF INTEREST

The authors declare no conflict of interest requiring disclosure in this article.

REFERENCES

1. Karacan, R., Mukhtarov, S., Barış, İ., İşleyen, A., and Yardımcı, M.E., *Energies*, 2021, vol. 14, p. 2947. https://doi.org/10.3390/en14102947
2. Nabipour, M., Escrochi, M., Ayatollahi, S., Boukadi, F., Wadhahi, M., Maamari, R., and Bemani, A., *J. Pet. Sci. Eng*., 2007, vol. 55, pp. 74–82. https://doi.org/10.1016/j.petrol.2006.04.013
3. Esene, C., Rezaei, N., Aborig, A., and Zendehboudi, S.C., *Fuel*, 2019, vol. 237, pp. 1086–1107. https://doi.org/10.1016/j.fuel.2018.08.106
4. Lake, L.W., Johns, R., Rossen, B., and Pope, G., *Soc. Petrol. Eng*., 2014, p. 496. https://doi.org/10.2118/9781613993286
5. Alvarado, V. and Manrique, E., *Energies*, 2010, vol. 3, pp. 1529–1575. https://doi.org/10.3390/en3091529
6. Speight, J.G., *Enhanced Recovery Methods for Heavy Oil and Tar Sands*, Gulf Publishing Company, Houston, Texas, 2013. https://doi.org/10.1016/C2013-0-15525-0
7. Massarweh, O. and Abushaikha, A.S., *Petroleum*, 2022, vol. 8, pp. 291–317. https://doi.org/10.1016/j.petlm.2021.05.002
8. Núñez-López, V. and Moskal, E., *Front. Clim*., 2019, vol. 1. https://doi.org/10.3389/fclim.2019.00005
9. Tan, Y., Li, Q., Xu, L., Ghaffar, A., Zhou, X., and Li, P., *Fuel*, 2022, vol. 328, p. 125256. https://doi.org/10.1016/j.fuel.2022.125256
10. Cruz, A.A., Amaral, M., Santos, D., Palma, A., Franceschi, E., Borges, G.R., Coutinho, J.A.P., Palácio, J., and Dariva, C., *J. Supercrit. Fluids*, 2019, vol. 143, pp. 24–31. https://doi.org/10.1016/j.supflu.2018.08.005
11. Dashti, H., Zanganeh, P., Kord, S., Ayatollahi, S., and Amiri, A., *Fuel*, 2020, vol. 262, p. 116615. https://doi.org/10.1016/j.fuel.2019.116615
12. Wang, P., Zhao, F., Hou, J., Lu, G., Zhang, M., and Wang, Z., *Energies*, 2018, vol. 11, p. 2483. https://doi.org/10.3390/en11092483
13. Rodriguez-Reartes, S.B., Cismondi, M., Franceschi, E., Corazza, M.L., Oliveira, J.V., and Zabaloy, M.S., *J. Supercrit. Fluids*, 2009, vol. 50, pp. 193–202. https://doi.org/10.1016/j.supflu.2009.06.017
14. da Silva, V.M., do Carmo, R.P., Fleming, F.P., Daridon, J.-L., Pauly, J., and Tavares, F.W., *Fluid Phase Equilib*., 2018, vol. 463, pp. 114–120. https://doi.org/10.1016/j.fluid.2018.01.029
15. Jaramillo, W.A.G., da Silva, V.M., do Carmo, R.P., Braga, A.J.O., Ndiaye, P.M., and Tavares, F.W., *Fluid Phase Equilib*., 2020, vol. 526, p. 112802. https://doi.org/10.1016/j.fluid.2020.112802
16. Eniolorunda, O.V., Chapoy, A., and Burgass, R., *Energy Fuels*, 2021, vol. 35, pp. 3731–3741. https://doi.org/10.1021/acs.energyfuels.0c02977
17. Hosseinipour, A., Japper-Jaafar, A.B., and Yusup, S., *Proc. Eng*., 2016, vol. 148, pp. 1022–1029. https://doi.org/10.1016/j.proeng.2016.06.580
18. Sasaki, K., Inayoshi, N., and Tashiro, K., *J. Phys. Chem. C*, 2009, vol. 113, pp. 3287–3291. https://doi.org/10.1021/jp809864m
19. Gur'eva, S.A., Marikhin, V.A., Myasnikova, L.P., Volchek, B.Z., and Medvedeva, D.A., *J. Phys. Conf. Ser*., 2019, vol. 1400, p. 055040. https://doi.org/10.1088/1742-6596/1400/5/055040
20. Ryu, M., Romano, M., Batsale, J.C., Pradere, C., and Morikawa, J., *Quant. Infrared Thermogr. J*., 2017, vol. 14, pp. 154–163. https://doi.org/10.1080/17686733.2016.1234672
21. Ewing, A.V., Gabrienko, A.A., Semikolenov, S.V., Dubkov, K.A., and Kazarian, S.G., *J. Phys. Chem. C*, 2015, vol. 119, pp. 431–440. https://doi.org/10.1021/jp510208e
22. Gabrienko, A.A., Martyanov, O.N., and Kazarian, S.G., *Energy Fuels*, 2016, vol. 30, pp. 4750–4757. https://doi.org/10.1021/acs.energyfuels.6b00718
23. Shalygin, A.S., Nesterov, N.S., Prikhod'ko, S.A., Adonin, N.Y., Martyanov, O.N., and Kazarian, S.G., *J. Mol. Liq*., 2020, vol. 315, p. 113694. https://doi.org/10.1016/j.molliq.2020.113694
24. Kovalev, E.P., Shalygin, A.S., Shubin, A.A., Kozhevnikov, I.V., Prikhod'ko, S.A., Adonin, N.Y., Kazarian, S.G., and Martyanov, O.N., *J. Mol. Liq*., 2022, vol. 348, p. 118082. https://doi.org/10.1016/j.molliq.2021.118082
25. Kazarian, S.G., *Appl. Spectrosc. Rev*., 1997, vol. 32, pp. 301–348. https://doi.org/10.1080/05704929708003318
26. Ewing, A.V. and Kazarian, S.G., *J. Supercrit. Fluids*, 2018, vol. 134, pp. 88–95. https://doi.org/10.1016/j.supflu.2017.12.011
27. Champeau, M., Thomassin, J.-M., Jérôme, C., and Tassaing, T., *J. Supercrit. Fluids*, 2014, vol. 90,

pp. 44–52.
https://doi.org/10.1016/j.supflu.2014.03.006
28. Coutinho, J.A.P. and Daridon, J.-L., *Pet. Sci. Technol*., 2005, vol. 23, pp. 1113–1128.
https://doi.org/10.1081/LFT-200035541
29. Zerbi, G., Magni, R., Gussoni, M., Moritz, K.H., Bigotto, A., and Dirlikov, S., *J. Chem. Phys*., 1981, vol. 75, pp. 3175–3194.
https://doi.org/10.1063/1.442490
30. Makarenko, S., Puchkovska, G., Kotelnikova, E., and Filatov, S., *J. Mol. Struct*., 2004, vol. 704, pp. 25–30.
https://doi.org/10.1016/j.molstruc.2004.01.046
31. Gupta, A.K., Brouwer, L., and Severin, D., *Pet. Sci. Technol*., 1998, vol. 16, pp. 59–69.
https://doi.org/10.1080/10916469808949772
32. Nivitha, M.R., Prasad, E., and Krishnan, J.M., *Mater. Struct*., 2019, vol. 52, p. 7.
https://doi.org/10.1617/s11527-018-1308-7
33. Ding, H. and Hesp, S.A.M., *Fuel*, 2020, vol. 277, p. 118220.
https://doi.org/10.1016/j.fuel.2020.118220
34. Kazarian, S.G., Vincent, M.F., Bright, F.V., Liotta, C.L., and Eckert, C.A., *J. Am. Chem. Soc*., 1996, vol. 118, pp. 1729–1736.
https://doi.org/10.1021/ja950416q
35. Gabrienko, A.A., Ewing, A.V., Chibiryaev, A.M., Agafontsev, A.M., Dubkov, K.A., and Kazarian, S.G., *Phys. Chem. Chem. Phys*., 2016, vol. 18, pp. 6465–6475.
https://doi.org/10.1039/c5cp06431g
36. Roehner, R.M. and Hanson, F.V., *Energy Fuels*, 2001, vol. 15, pp. 756–763.
https://doi.org/10.1021/ef010016q
37. Snyder, R.G., Maroncelli, M., Strauss, H.L., and Hallmark, V.M., *J. Phys. Chem.*, 1986, vol. 90, pp. 5623–5630.
https://doi.org/10.1021/j100280a030
38. Oh, K., , Patent USA 8326548 B2, 2011.
39. Harrick, N.J., *Internal Reflection Spectroscopy*, New York: Wiley, 1967.